Virtual Neurons

3D-reconstructions of neurons

Manos Papadakis
University of Houston

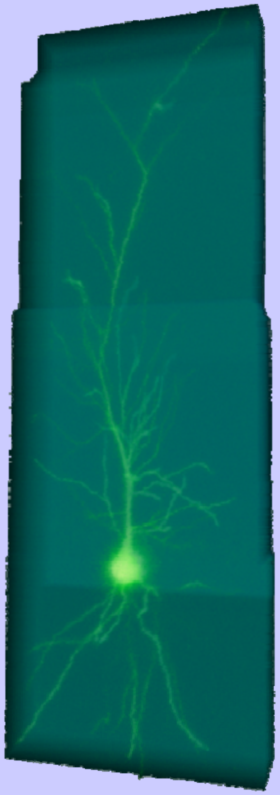

Collaborators

I. Kakadiaris,
D. Labate

Neuroscience/data acquisition collaborators:
P. Saggau (BCM) and F. Laenza (UTMB)

D. Jimenez, P. Hernadez-Herrera and A. Santamaria-Pang

Morphological reconstruction of neurons: significance

- To understand the I/O relationship of individual central neurons
  - Combining detailed structural and functional information

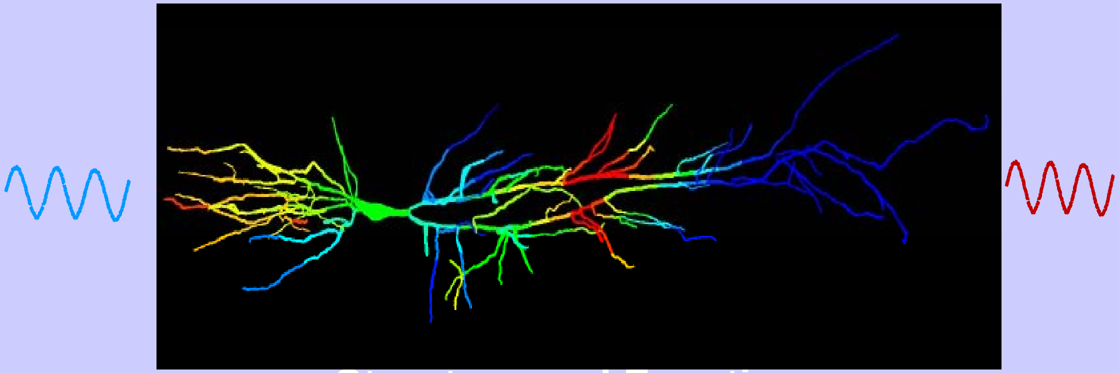

Image Analysis Goal:

- Extract the geometric properties of dendritic arbors
- Reconstruct a computer-generated 3D-image of the arbor.

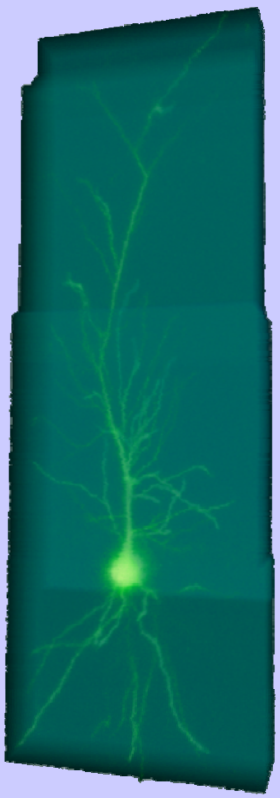

Raw Data

Reconstruction

Do the last task when a neuron is activated and responds.

This will help add a layer of a true activation/response model.

Characteristics of the dendritic structure

– Global features (e.g., branch size, shape, and tapering; branch bifurcations; overall geometry, distribution of the shape of spines)

– Local features (e.g., the dendritic spines)

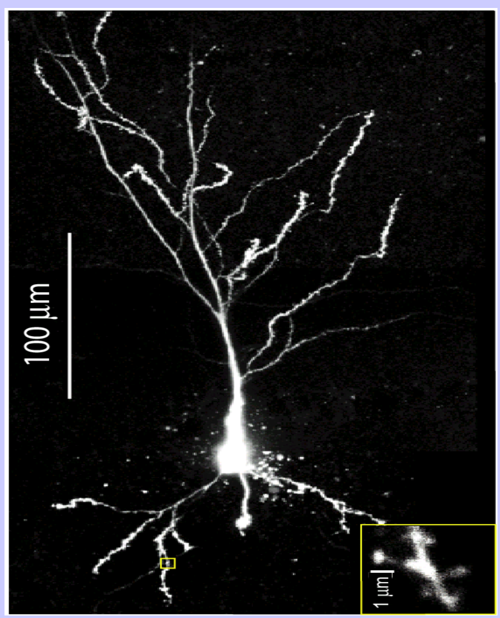

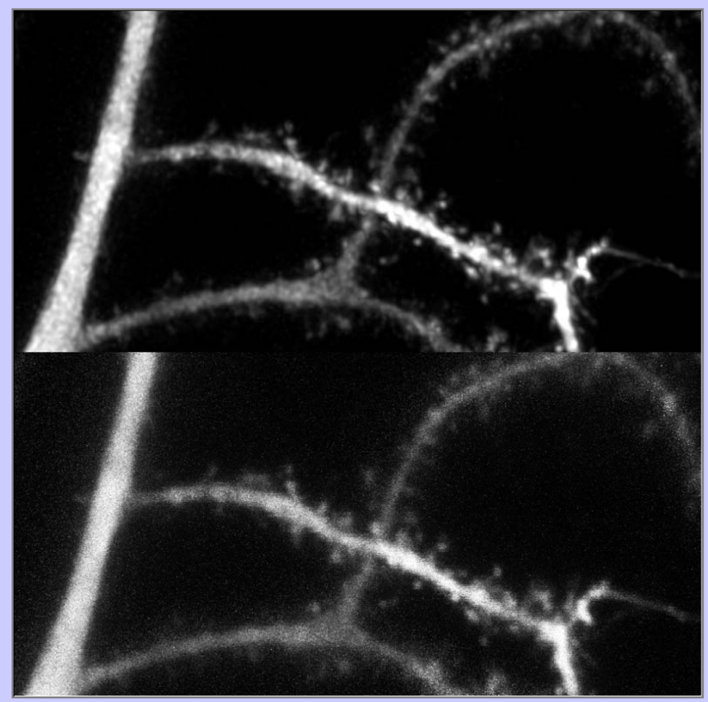

Challenges (1)

- Uneven distribution of the fluorescent dye.
- Depth-dependent intensity changes and scattering

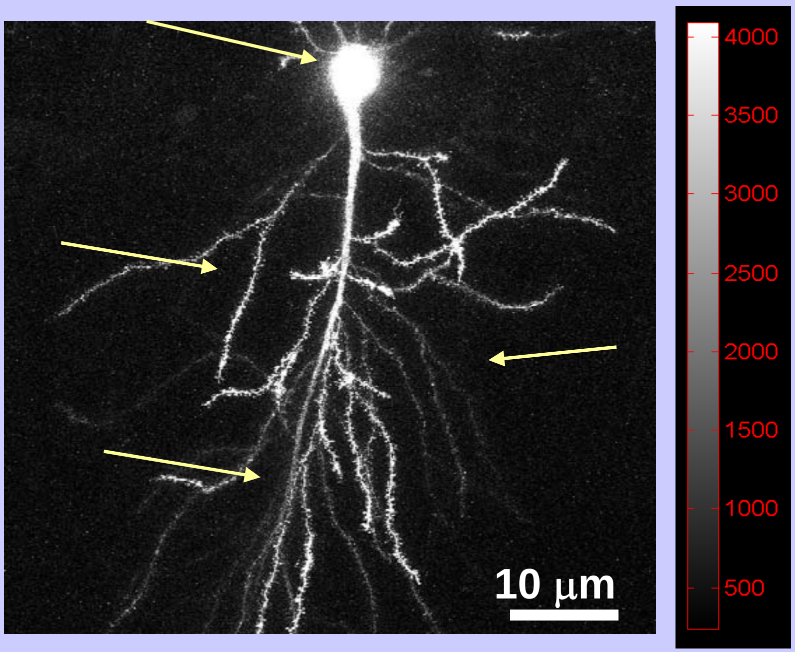

x –y maximum intensity projection

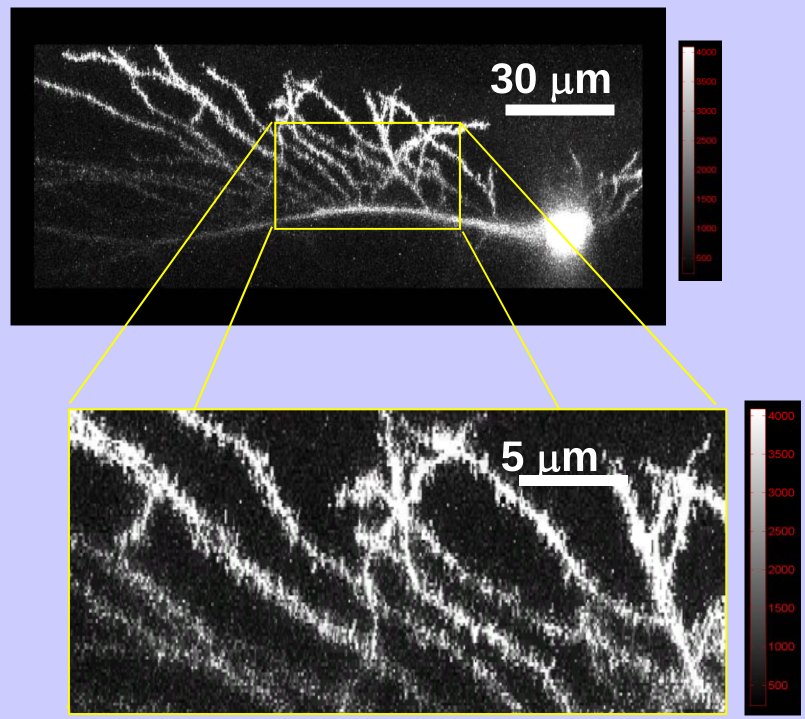

y –z maximum intensity projection

Challenges (2)

- Irregular shape of the dendrites
- Adjoining structures: spines
- Many features of interest are at the resolution limit of light microscopy

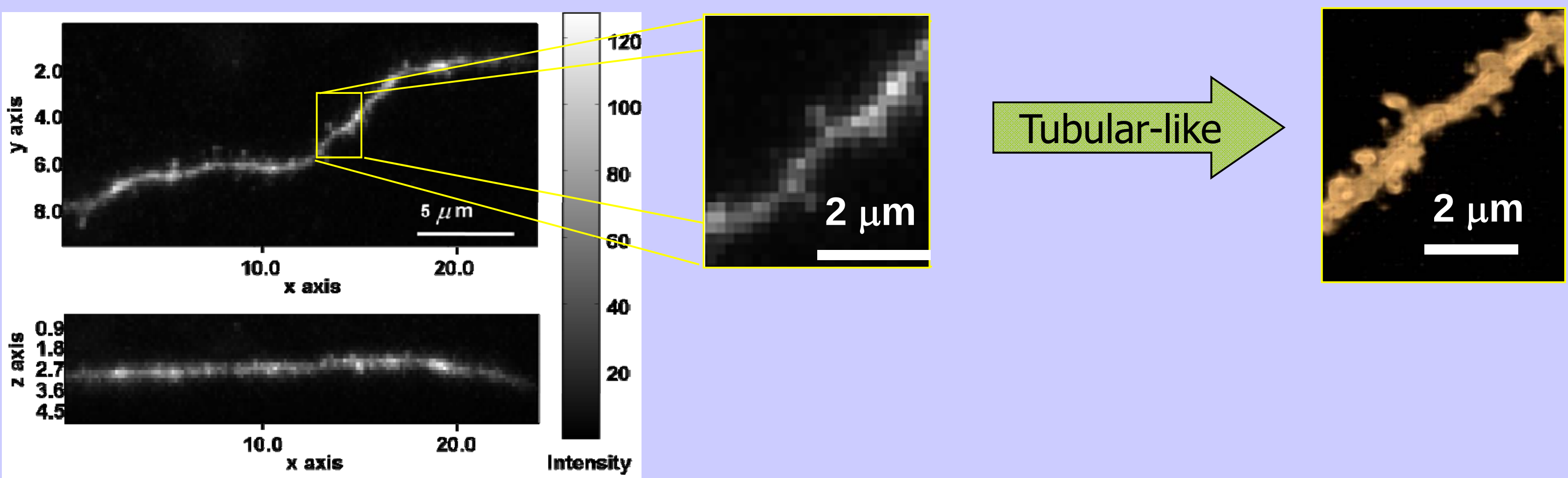

Challenges (3)

- Low signal to noise ratio: thermal noise, photon shot noise
- Different noise model (Poisson) from CT or MRI (Gaussian)

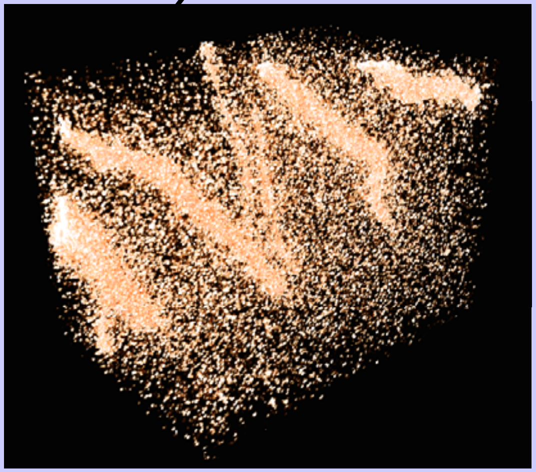

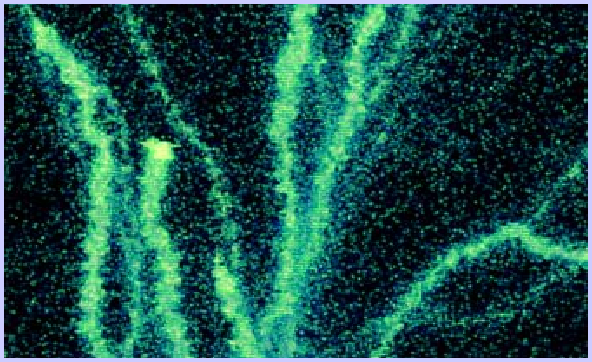

ORION 1 Morphological Reconstruction Pipeline

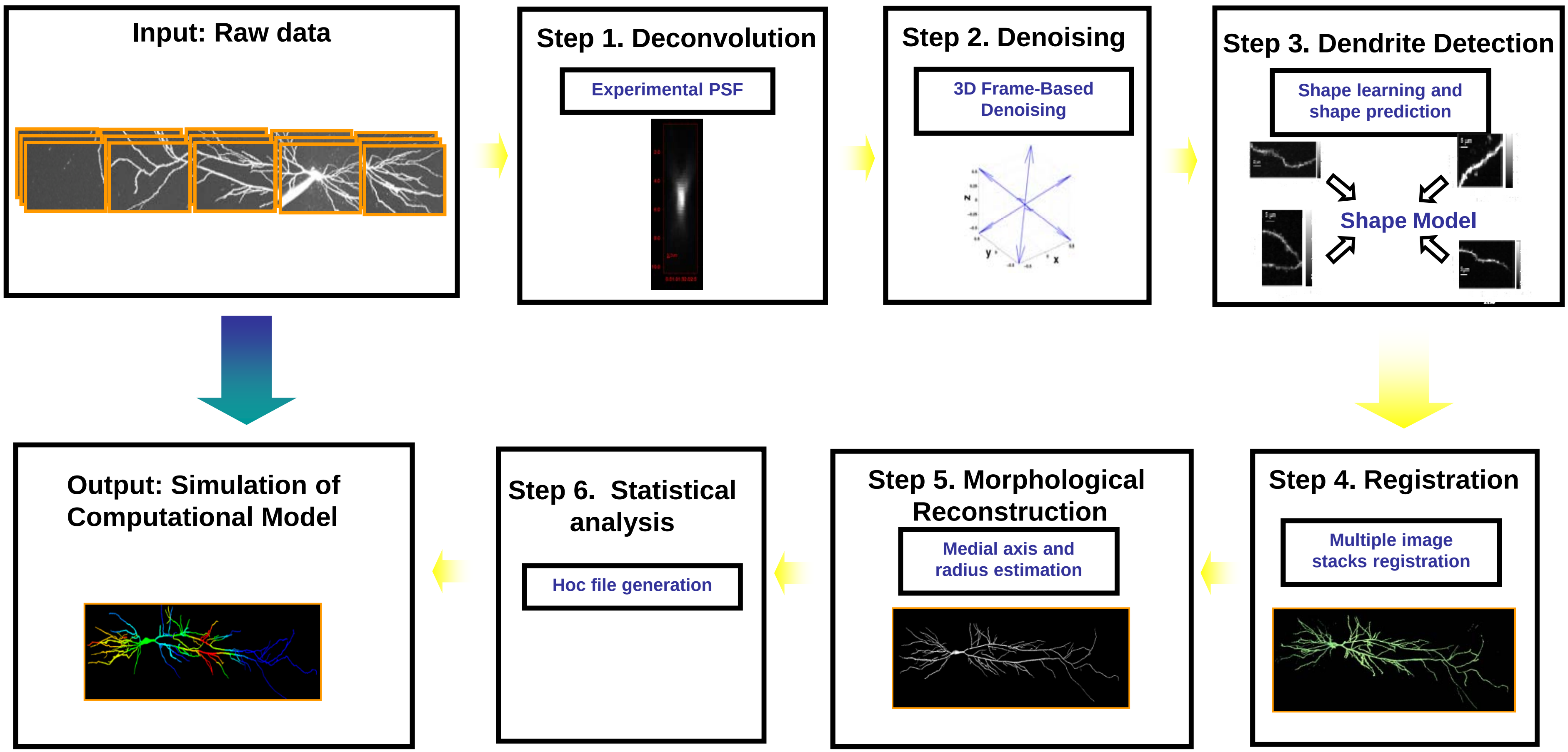

Dendrite Detection: Shape Features

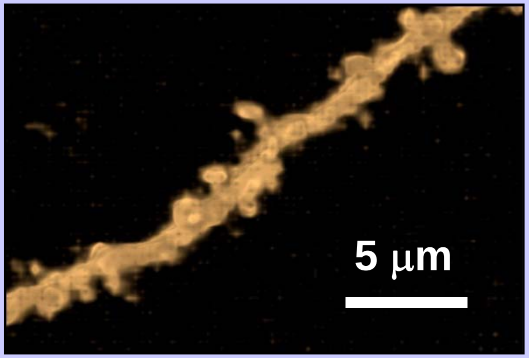

- Filter the 3D-image I with Gaussian kernels G_σ for different σ.
- Extract the Hessian of $I * G_\sigma(\mathbf{x})$
- Find the eigenvalues of $I * G_\sigma(\mathbf{x})$.

These are the shape features.

- Classification of voxels according to the learned features.

Dendrite Detection: Learning from Examples

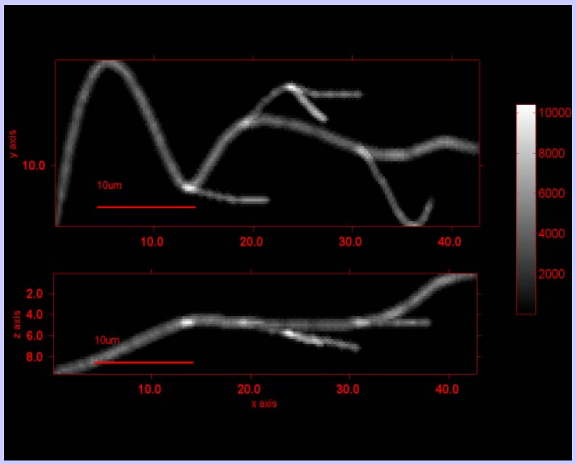

Model to Learn

Shape Learning

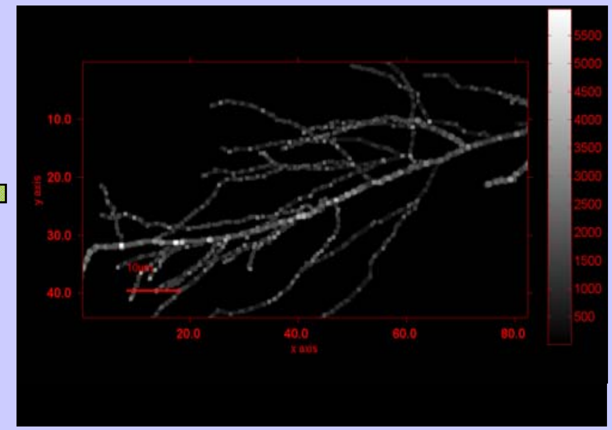

Data to predict

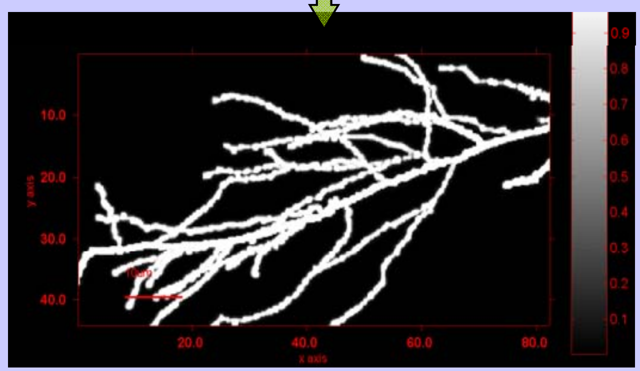

Prediction

Dendrite Detection: Comparisons

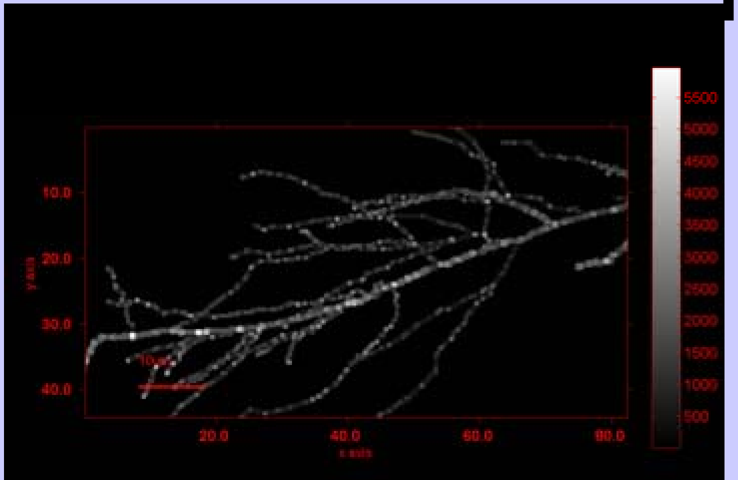

Original Data

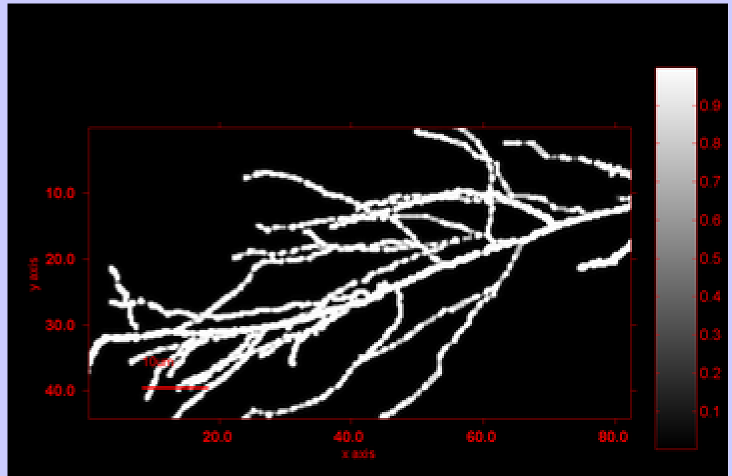

Orion 1

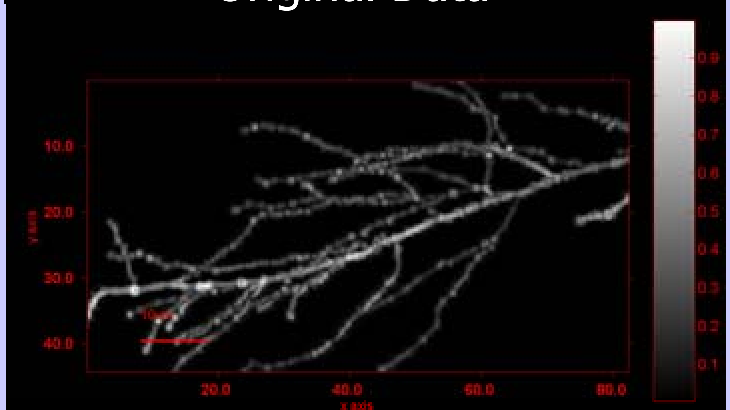

Frangi

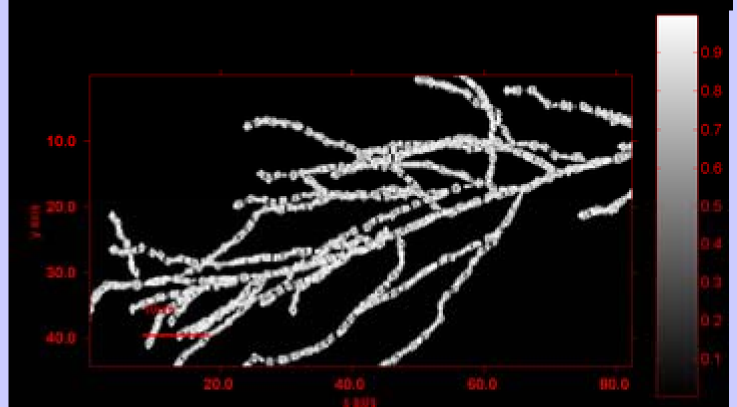

Sato

Results (2)

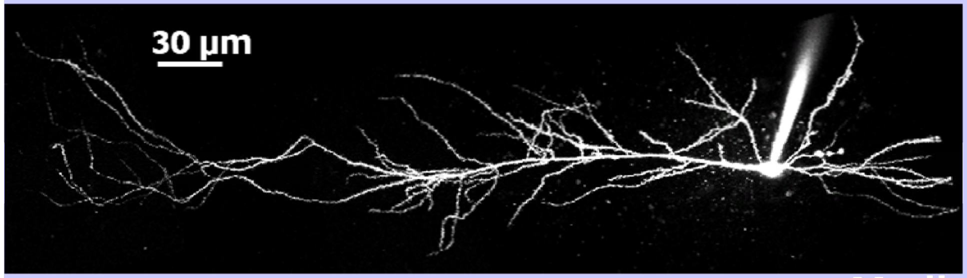

Medium

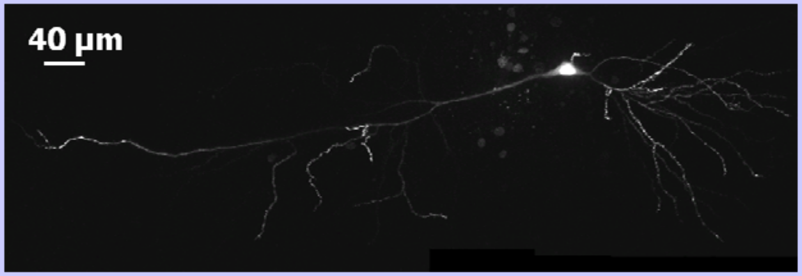

Poor

Results (3)

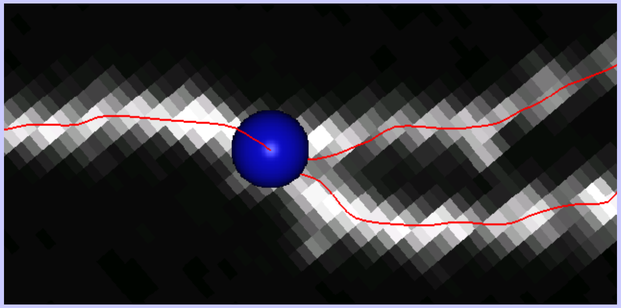

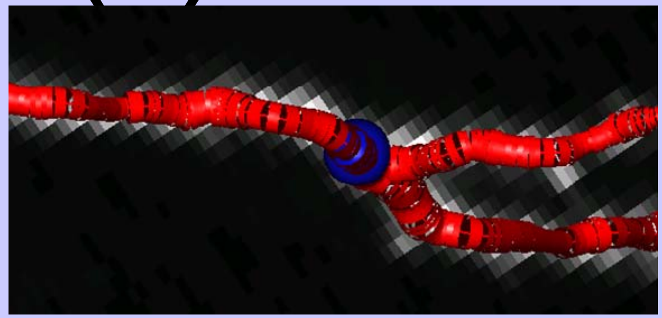

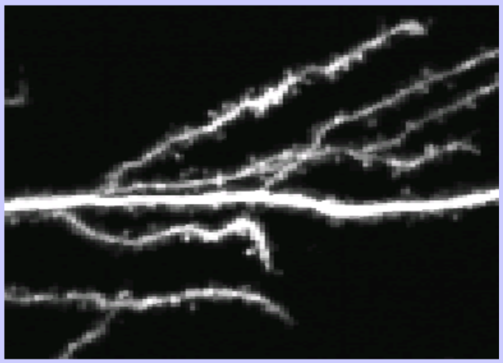

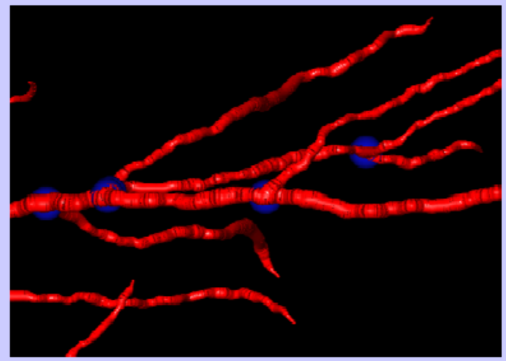

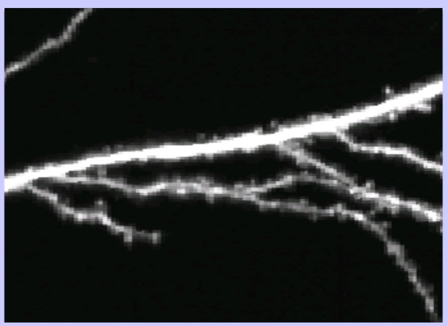

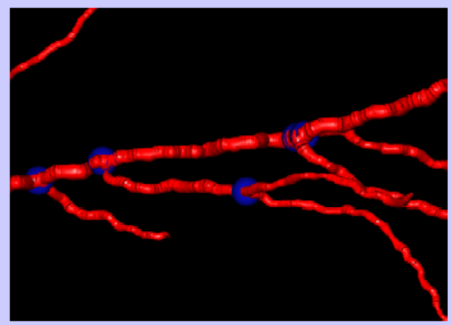

Orion 1 Reconstruction for Diadem Data Set 1

Volume 1: CF1

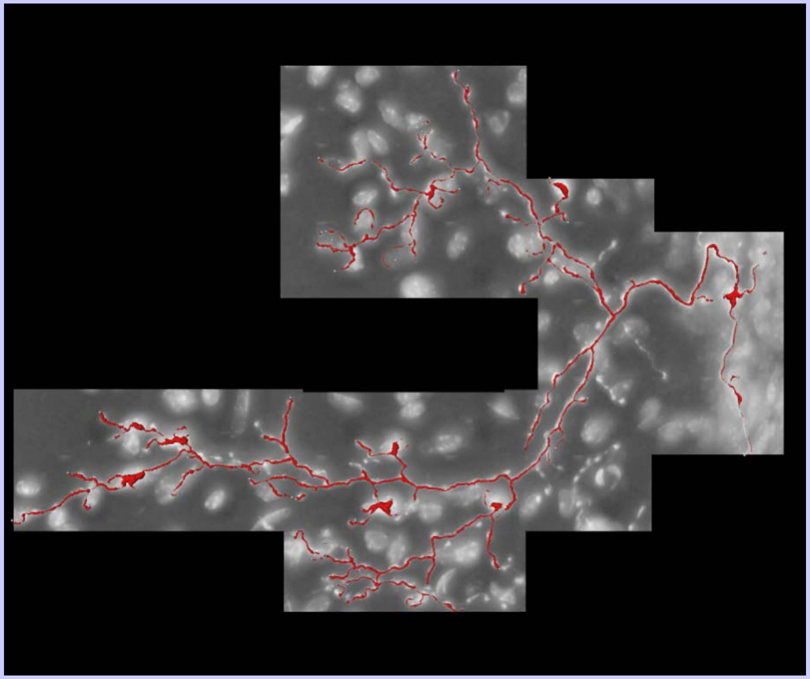

Volume 2: CF2

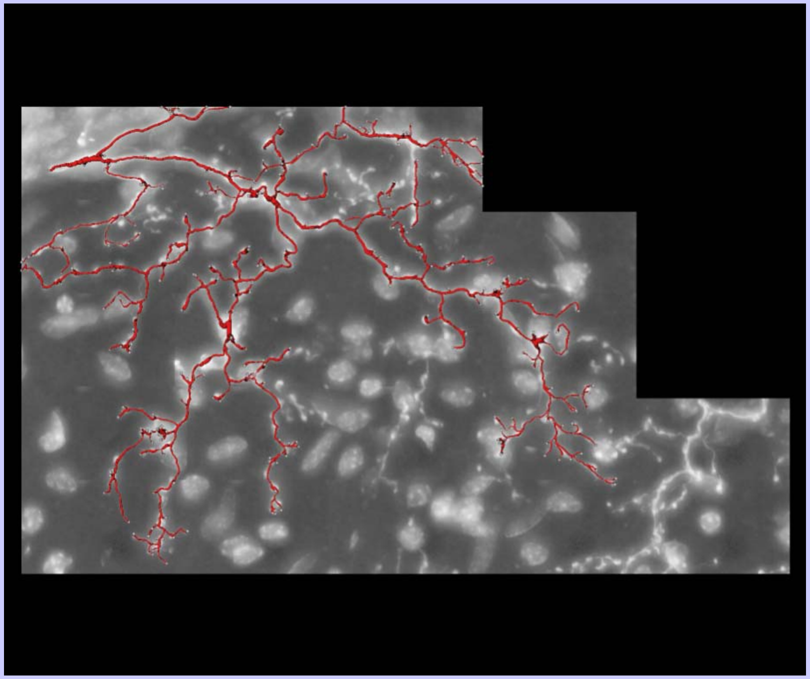

Orion 1 Reconstruction for Diadem Data Set 5

Volume 1: OP1

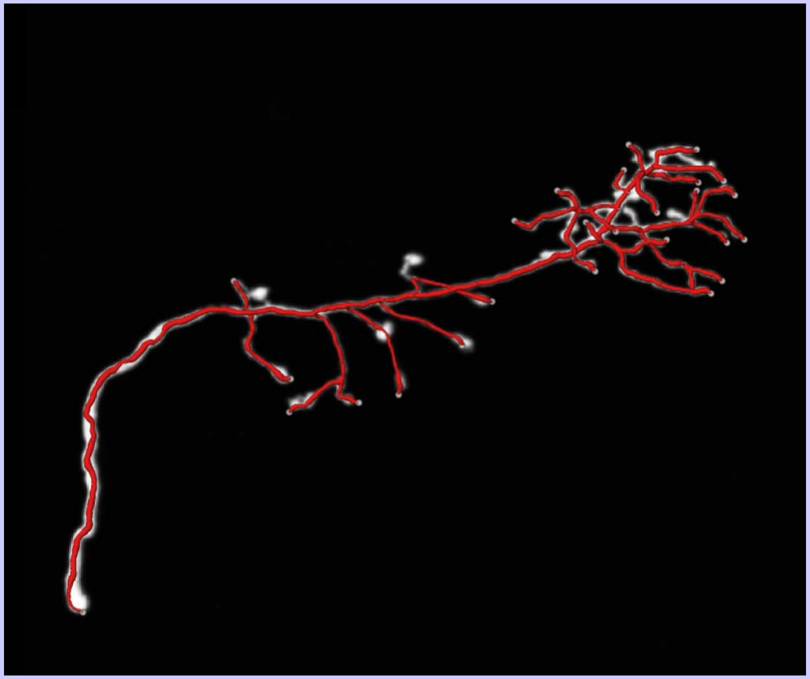

Volume 3: OP3

Orion 1 Reconstruction for Diadem Data Set 2

Raw data

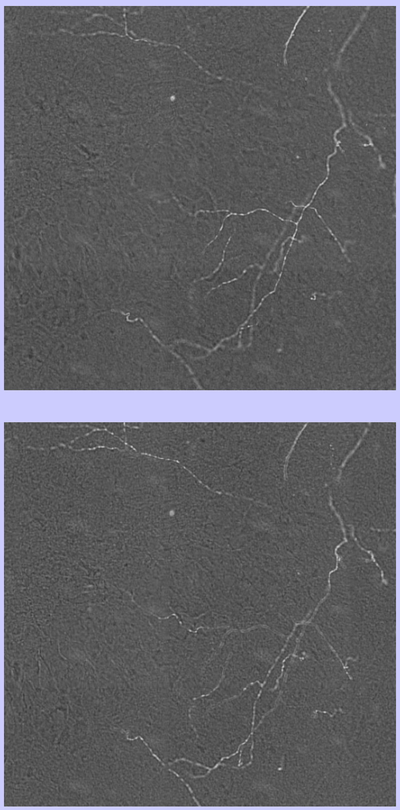

Prediction

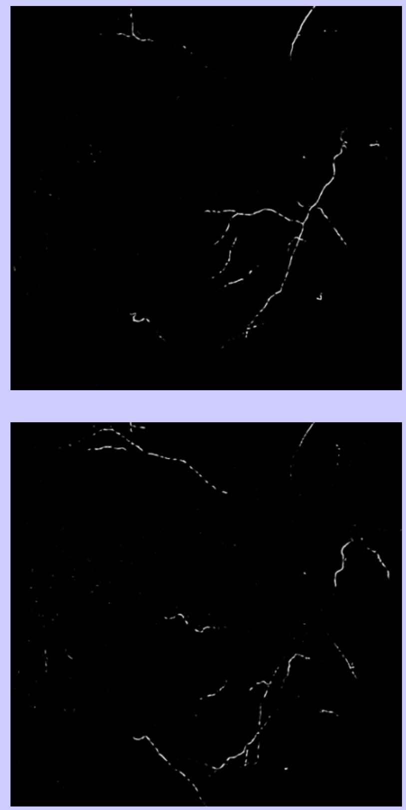

Synthetic data volumes

- Synthetic data volumes can be used for benchmarking imaging algorithms in neuroscience.
- These algorithms aim to extract the geometric characteristics of a neuron from the input 3D-image.
- Benchmarking of their performance must be done under ideal conditions where the ground truth is precisely known.
- Neurons can be modeled as tubular structures.

Simple tube model: R rotation (in) $SO(3)$

$T_a f(x) = f(x-a)$, $x \in \mathbb{R}^3$.

Take $t(x_1, x_2, x_3) = A e^{-\frac{x_1^2}{2\sigma_1^2}} e^{-\frac{x_2^2+x_3^2}{2\sigma_2^2}}$

A simple tube is $T_a R t_{\sigma_1,\sigma_2}$

A neuron can be modeled (approximately) as

$$\sum_{i=1}^{2} \sum_{\sigma_i \in S_i} \sum_{a \in J} \sum_{R \in I} T_a R t_{\sigma_1, \sigma_2}$$

$J \subset \mathbb{R}^3$

I subset of $SO(3)$.

Typically t_{σ_1,σ_2} will have $\sigma_2 << \sigma_1$

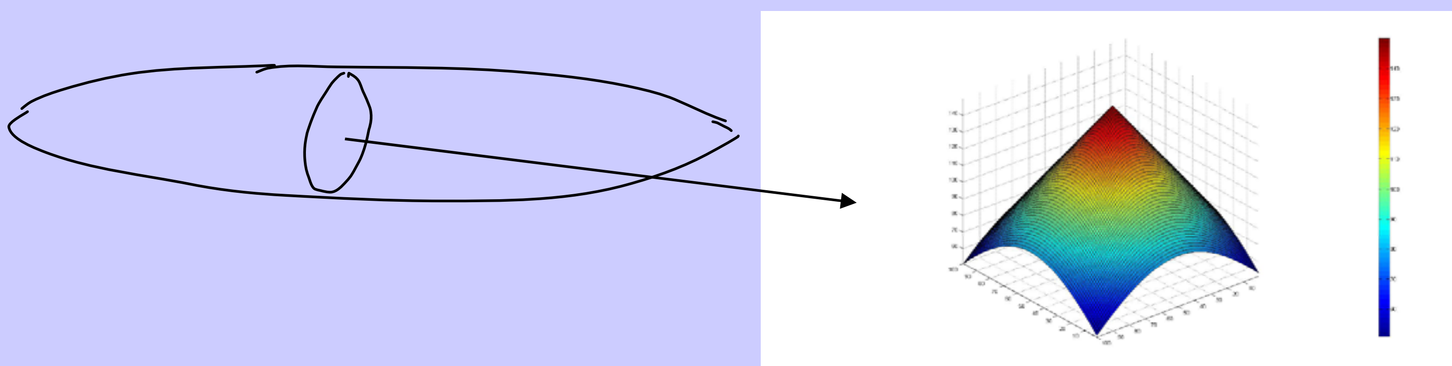

Analog to digital in multidimensions

f band-limited and in $L^2(\mathbb{R}^d)$, $f \in PW_\Omega$, $\Omega \subseteq \mathbb{R}^d$

Suppose $\mathcal{M}$ is a group of orthogonal transforms acting on $\mathbb{R}^d$, e.g. rotations, shearing operators

$\rho(M) f(x) = f(Mx)$, $M \in \mathcal{M}$ $\quad (\rho(M) f)^\wedge(\xi) = \hat{f}(M\xi)$

Take $\Omega \subseteq \mathbb{T}^d$, $(d=2)$ $\Omega \subseteq [-\frac{1}{2}, \frac{1}{2}]^2$

PW_Ω remains invariant under the action of $\rho(\mathcal{M})$ if $M(\Omega) \subseteq \Omega$ for all $M \in \mathcal{M}$

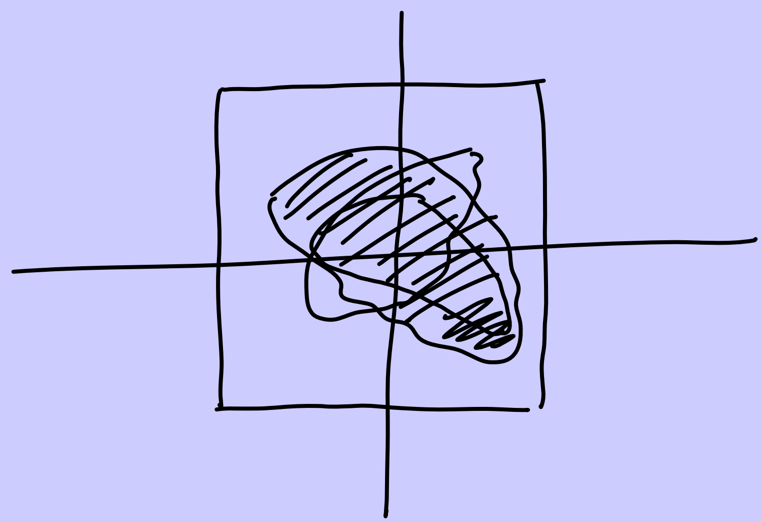

Joint with D. Jimenez and D. Labate

For $\mathcal{M} = SO(d)$ Ω must be radial. Then, the sampling rate of f does not change.

Theorem (Romero, Jain, Alexander, Baid, P) If V is invariant under shifts, $\tau_n(V) \subseteq V$, $\tau_n f(x) = f(x-n)$ and $\rho(R)(V) \subseteq V$ for all rotations R, then $V = PW_\Omega$, Ω is radial.

Take radial $\Omega \subseteq [-\frac{1}{2}, \frac{1}{2}]^d$, $f \in PW_\Omega$

$$f = \sum_n \langle f, \tau_n \phi \rangle \tau_n \phi \qquad \hat{\phi} = \chi_\Omega$$

$\{\tau_n \phi : n\}$ is a Parseval frame of PW_Ω.

ϕ has bad decay. $\longleftarrow$ Ooops!!

Analysis $\quad A(f) = \{\langle f, \tau_n \phi\rangle\}_n$ samples $(A \to D)$

Synthesis : $\quad \sum_n \langle f, \tau_n \phi\rangle \tau_n \phi \qquad D \to A$ reconstruction.

$\boxed{\text{Filter design}}$

$$\updownarrow$$

$$\underbrace{\left(\sum_n \langle f, \tau_n \phi\rangle e^{-2\pi i n\cdot\xi}\right)\chi_\Omega(\xi)}_{\hat f \chi_\Omega = \hat f}$$

recall $\hat f$ vanishes outside Ω.

Smooth-out χ_Ω

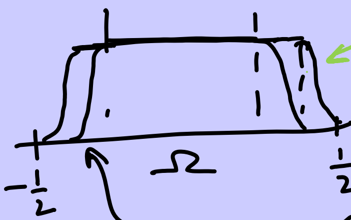

$\hat\phi_s$ smooth improves interpolation

$\hat\phi_a$ smooth improves analysis as we will see

$$\hat f = \hat f \chi_\Omega = \hat f\, \overline{\hat\phi_a}$$

Nyquist oversampling

$$\langle f, \tau_n \phi_a\rangle = \int \hat f(\xi)\, \overline{\hat\phi_a(\xi)\, e^{-2\pi i n\cdot\xi}}\, d\xi$$

$\mathbb{Z}^2$-periodic

So the sampling kernel is ϕ_a with good spatial localization

Reconstruction : $\quad \hat f = \hat f\, \overline{\hat\phi_a} = (\underbrace{\hat f\, \overline{\hat\phi_a}}_{=})\, \hat\phi_s = \mu\, \hat\phi_s$

So $$f = \sum_{n \in \mathbb{Z}^d} \langle f \;\; \tau_n \phi_a \rangle \, \tau_n \phi_s$$

In a practical application we restrict $n \in \Lambda$ finite subset of $\mathbb{Z}^d$. Typically $\Lambda = [-N_1, N_1] \times [-N_2, N_2]$ (linear approximation) or the best approximation with $N = (2N_1+1) \times (2N_2+1)$ terms. Also of interest is

$\| f - f_\Lambda \|_\infty$ or in a Sobolev norm

where $$f_\Lambda = \sum_{n \in \Lambda} \langle f, \tau_n \phi_a \rangle \, \tau_n \phi_s$$ L_2-convergence

$$\| f - f_\Lambda \|_\infty \le \underset{\substack{\uparrow \\ \text{not depending on } f}}{K} \sum_{n \notin \Lambda} | \langle f, \tau_n \phi_a \rangle |$$

Given a group or orthogonal transformations $\mathcal{M}$ what is
$e(M) = \| \rho(M) f - (\rho(M) f)_\Lambda \|_\infty$.

$$e(M) = \| \rho(M) f - (\rho(M) f)_\Lambda \|$$ ↖ suitable norm

Take $\{M_i\}$ converging to M. Assume $\mathcal{M}$ be a compact group. Then $\|\rho(M_i) f - \rho(M) f\|_p \longrightarrow 0$

with respect to all L^p norms.

$$(\rho(M_i) f)_\Lambda = \sum_{n \in \Lambda} \langle \rho(M_i) f, \tau_n \phi_a \rangle \tau_n \phi_s$$

finite

So $\| (\rho(M_i) f)_\Lambda - (\rho(M) f)_\Lambda \|_p \longrightarrow 0$

So $\| e(M_i) - e(M) \|_p \longrightarrow 0$, Thus $M \longmapsto e(M)$ is continuous

on $\mathcal{M}$ so it is bounded.

However, the upper bound is important if it is small or if e remains constant.

How big $\|\rho(M)f - (\rho(M)f)_\Lambda\|_\infty$ can be?

Example:

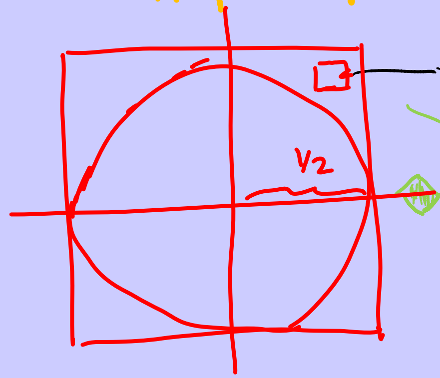

$\hat{h}$ smooth vanishes outside this little square.

$\hat{h}$-rotated by 45°.

$$\|h - h_\Lambda\|_\infty < \frac{\|h\|_\infty}{2}$$

for some Λ

$$\|\rho(\tfrac{\pi}{4})h - \underbrace{(\rho(\tfrac{\pi}{4})h)_\Lambda}_{=0}\|_\infty = \|h\|_\infty$$

$\uparrow$ for all Λ

M = rotation by $\pi/4$

Wire Sampling, Wire = Our work in progress (Jimenez, Labate & P)

Take R rotations in $SO(d)$, take $d=2$ for simplicity

$$\|\rho(R)f - (\rho(R)f)_\Lambda\|_\infty \le K \sum_{n\notin\Lambda} |\langle \rho(R)f, \tau_n\phi_a\rangle|$$

ϕ_a radial

$\hat{\phi}_a$ C^∞

$$\langle \rho(R)f, \tau_n\phi_a\rangle = \int \hat{f}(R\xi)\,\overline{\hat{\phi}_a(\xi)}\,\overline{e^{-2\pi i n\cdot\xi}}\,d\xi =$$

$$\int \hat{f}(\xi)\,\overline{\hat{\phi}_a}(\xi)\,e^{2\pi i n\cdot(R\xi)}\,d\xi = \underbrace{(f * \tilde{\phi}_a)(R^T n)}$$

value of $(\hat{f}\,\overline{\hat{\phi}_a})^\vee$ at $R^T n$

$$\left|\langle \rho(R) f, T_n \Phi_a \rangle\right| \le \frac{\| D^b(\hat{f}\,\overline{\hat{\Phi}_a})\|_1}{|R^T n|^{|b|}} = \frac{\| D^b(\hat{f}\,\overline{\hat{\Phi}_a})\|_1}{|n|^{|b|}}$$

independent of R

So if Φ_a is radial of $\hat{\Phi}_a(\xi)=1$ for all $\xi \in B(0,b_0)$ where $\hat{f}(\xi)=0$ if $|\xi|>b_0$, $b_0<1/2$

then $\| \rho(R) f - (\rho(R) f)_\Lambda \|_\infty \le O\left(\sum_{n\notin\Lambda} \frac{1}{|n|^{|b|}}\right)$

- Is it true that if Φ_α is radial then a greedy algorithm selection of Λ for f is not influenced by the rotations of f?
- What happens with other orthogonal transform groups and other norms, e.g. Sobolev norms?

Changing resolution/superesolution

Changing resolution in images or creating crisp images from a series of low-resolution images is significant in forensic science and biometrics.

Artifacts/errors must not depend on the orientation of singularities.

$f \in V_j$ produce $\tilde{f} \in V_{j-1}$ projection of f onto V_{j-1}

$h \in V_{j-1}$ if and only if $h(2\,\cdot) \in V_j$

V_j principal shift-invariant, take $j=0$ for convenience

ϕ generator of $V_0 = \overline{\operatorname{span}}\{T_n \phi : n \in \mathbb{Z}^d\}$

$h \in V_0$, $\quad \hat{h}(\xi) = \mu(\xi)\,\hat{\phi}(\xi)$, $\xi \in \mathbb{R}^d$

periodic

$f \in V_0 \quad \hat{f}(\xi) = \mu(\xi)\,\hat{\phi}(\xi)$

$$\tilde{f}(\xi) = \tilde{\mu}(2\xi)\,\hat{\phi}(2\xi)$$

Find $\tilde{\mu}$ from μ.

We want

$$\operatorname{error}(M) = \| \rho(M) f - \widetilde{\rho(M) f} \| = \text{const.} \quad \text{for all } M \in \mathcal{M}$$

suitable norm

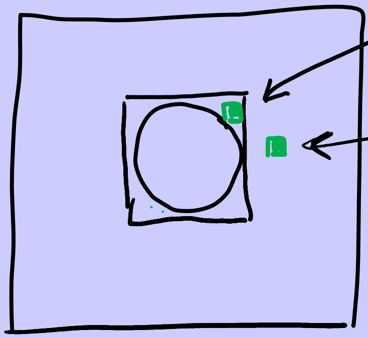

$\widehat{\tilde{f}} = \hat{f}$

$\rho(\frac{\pi}{4}) f$ but $\widetilde{\rho(\frac{\pi}{4}) f} = 0$

$\text{error}(\frac{\pi}{4}) = \| f \|$.

- If $V_0 = PW_\Omega$ and $M(\Omega) = \Omega$, then $V_{-1} = PW_{\Omega/2}$ and the projection onto $V_0 \ominus V_{-1} = W_{-1}$ commutes with all $\rho(M)$. Then

$$\text{error}(M) = \| \rho(M) f - \widetilde{\rho(M) f} \|_2 = \text{constant}. \qquad (*)$$

<u>Definition:</u> Orthogonal transform insensitive downsampling

If $(*)$ is valid, with respect to L^2 or to another suitable norm.

Isotropic Re-sampling

We wish to take a super-resolution or a sub-resolution using the IMRA framework.

- This is meant to preserve information in an isotropic fashion, i.e., without directional bias.
- Preliminary results show promise for optimal performance, particularly for super-resolution, using an IMRA setting.

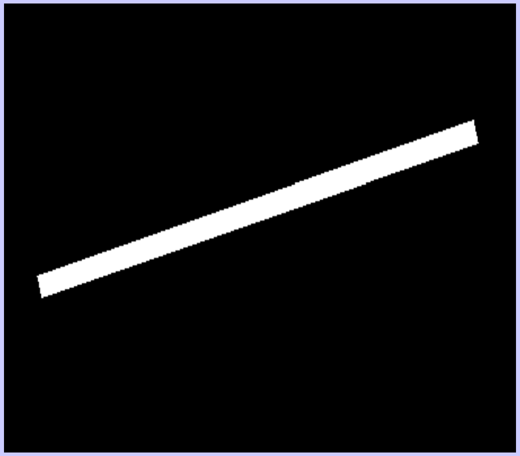

800 x 800

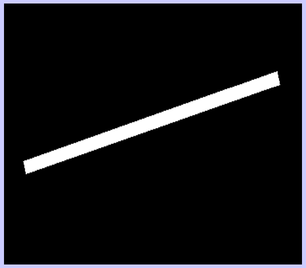

400 x 400

Isotropic Down-sampling

- Down-sampling in an IMRA framework for 15 degree rotation of a line e.g.,

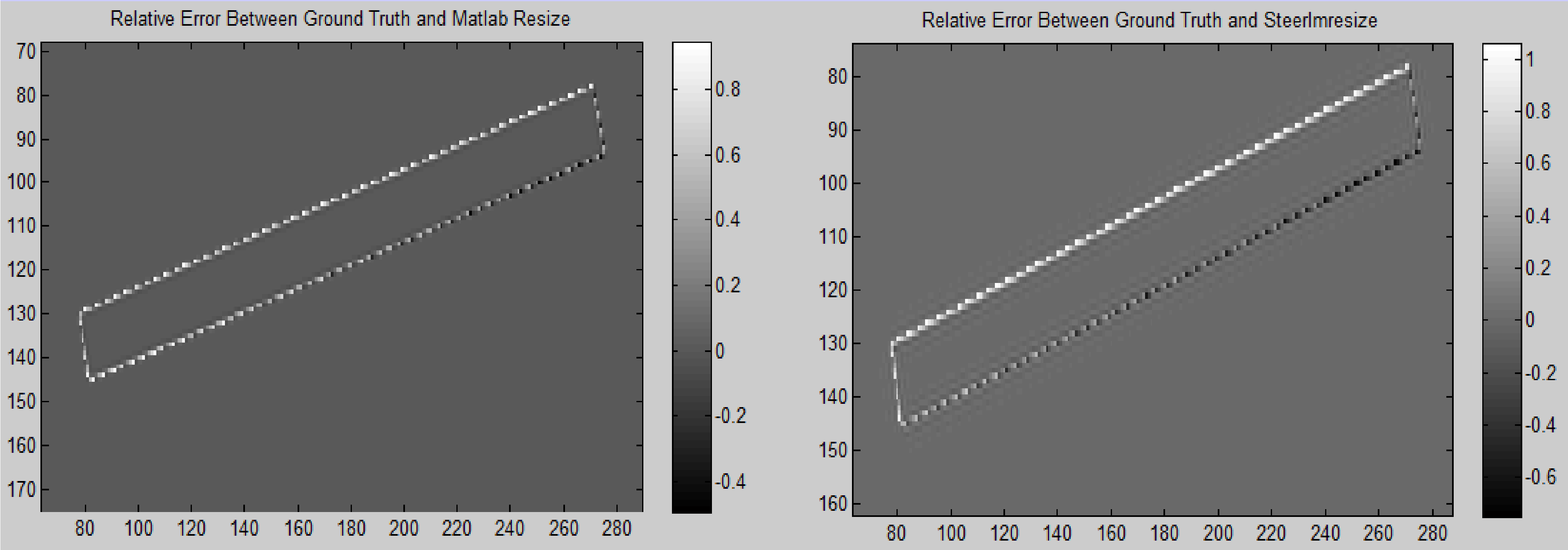

Isotropic Down-sampling

- Down-sampling in an IMRA framework for 45 degree rotation of a line e.g.,

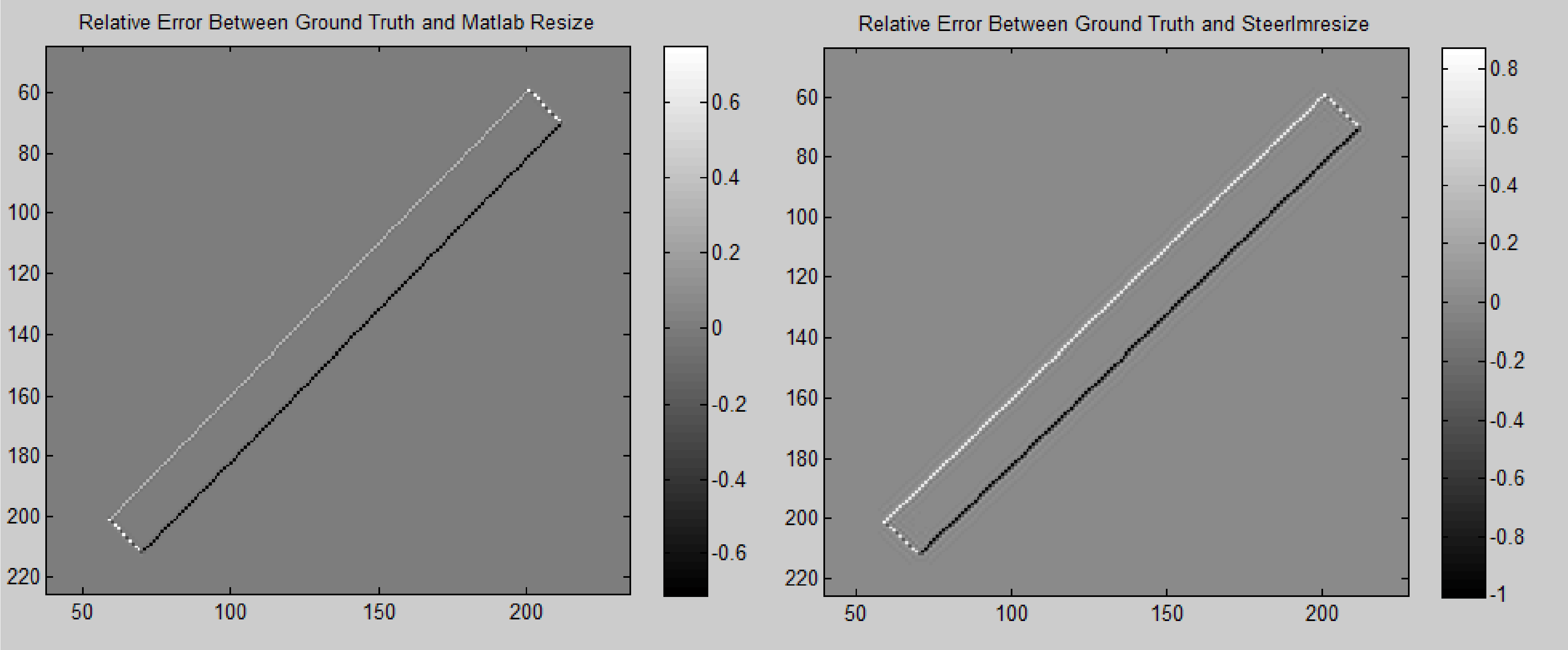

Isotropic Up-sampling

- Up-sampling in an IMRA framework for 15 degree rotation of a line e.g.,

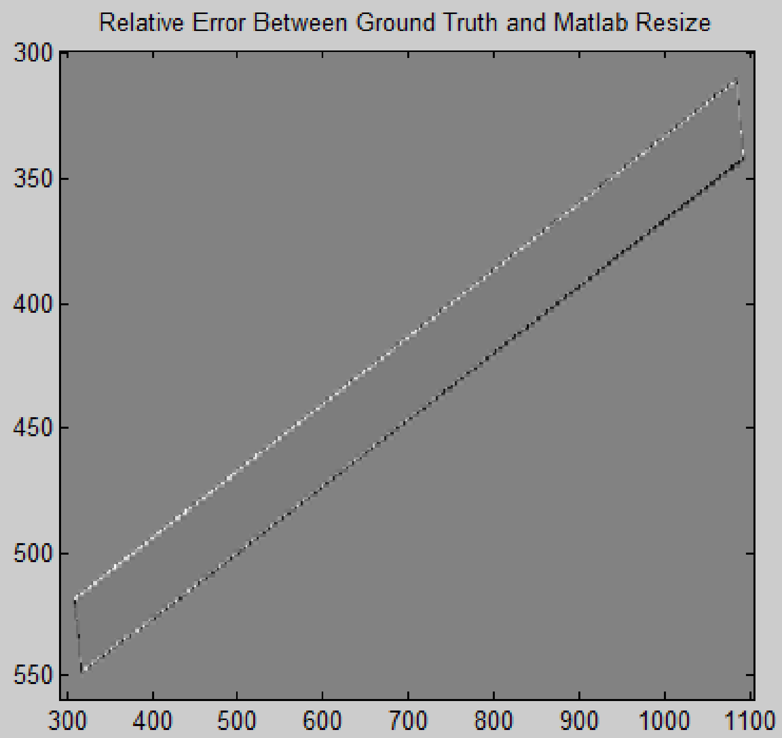

Isotropic Up-sampling

- Up-sampling in an IMRA framework for 45 degree rotation of a line e.g.,

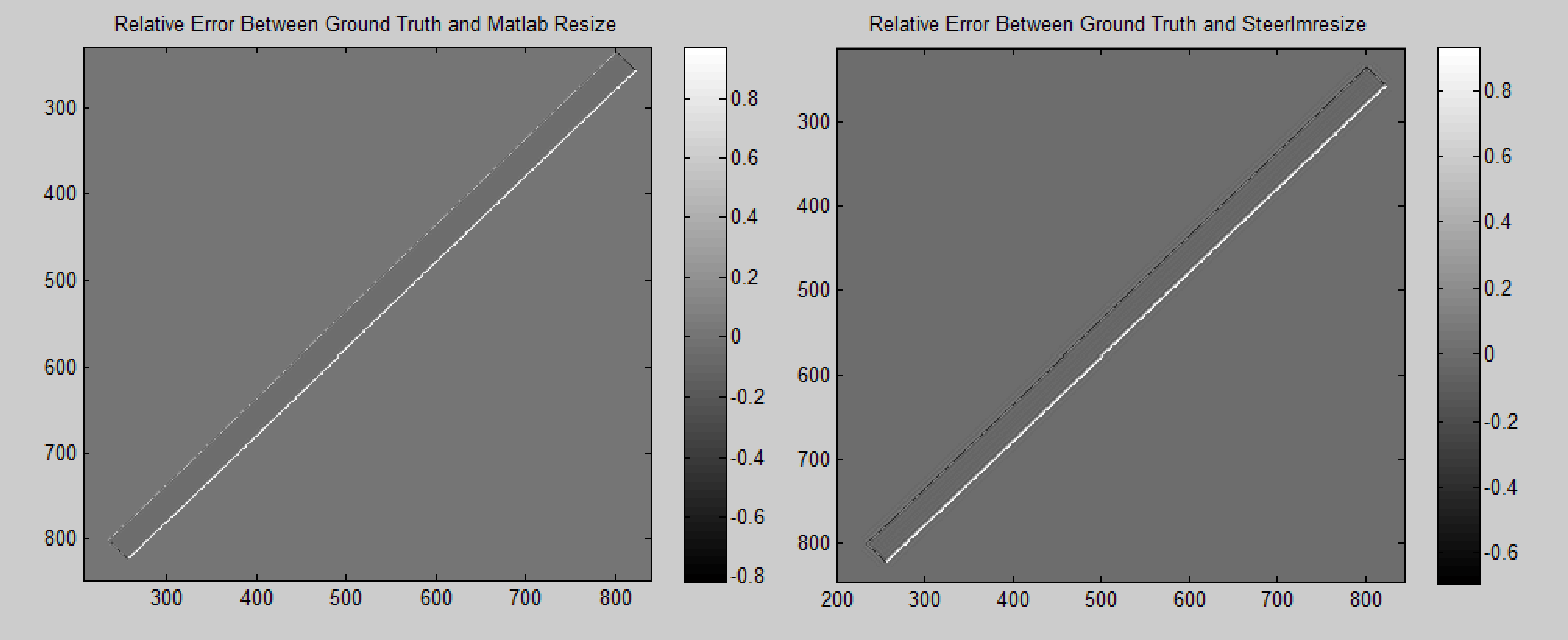

Examples of synthetic dendrites

Cylinder along the x-axis for sanity check

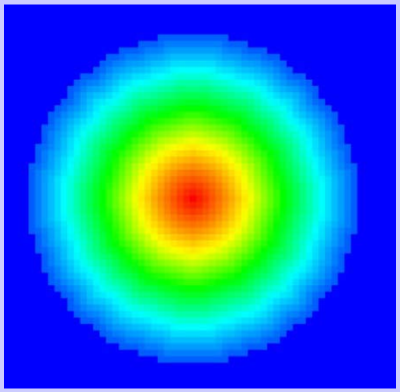

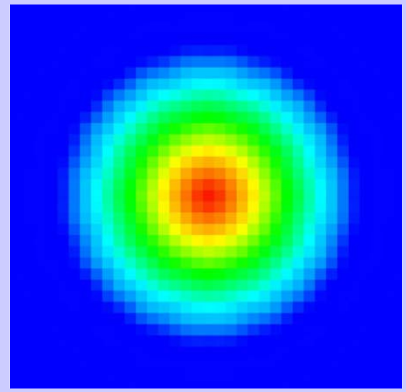

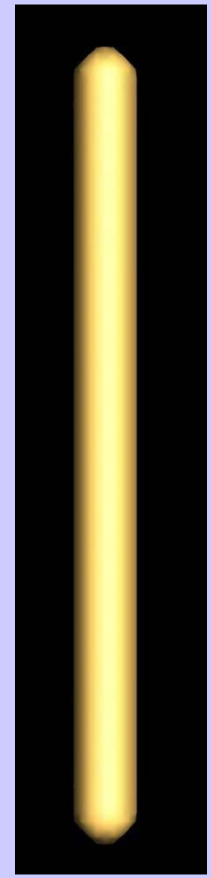

Second downsampling

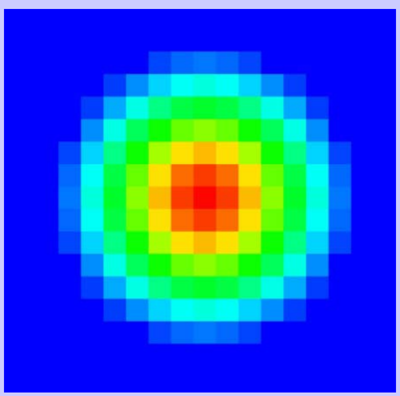

Third downsampling

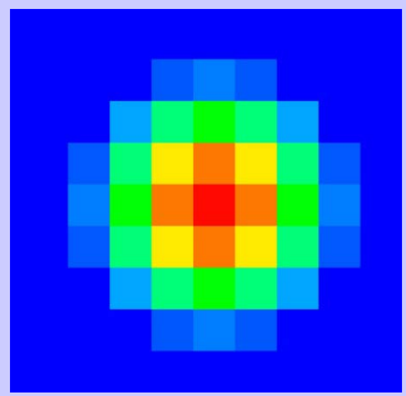

Examples of synthetic dendrites

- Cross section 30^o

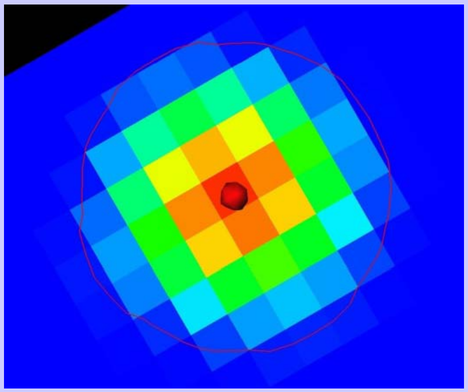

- Cross section 45^o

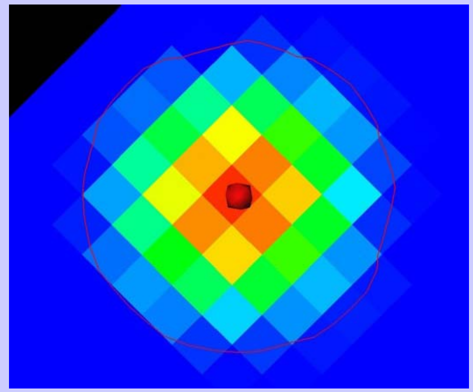

- Cross section 90^o

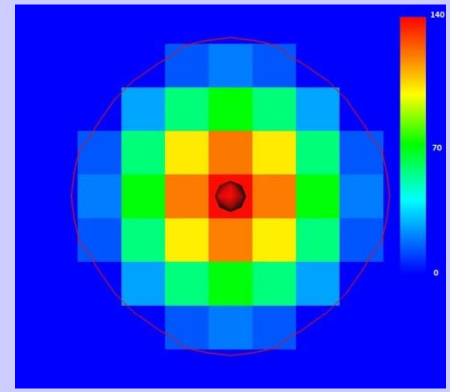

- Cross section 30^o

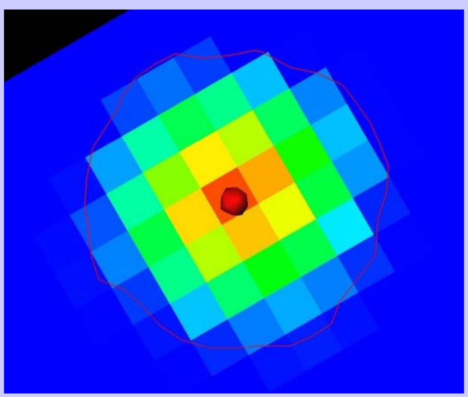

- Cross section 45^o

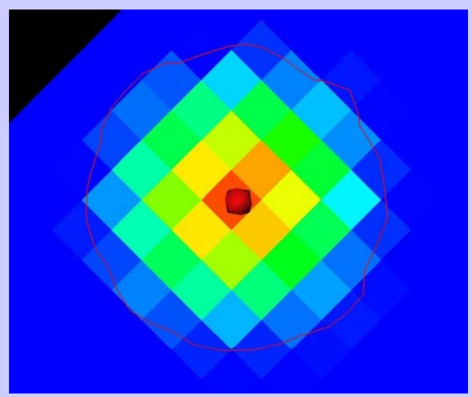

- Cross section 90^o

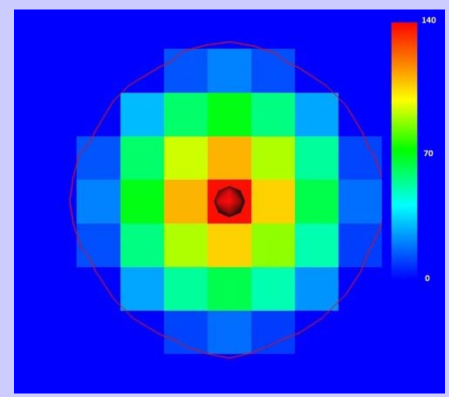

Examples of synthetic dendrites

- Slices at 30 º, 45 º, and 90 º

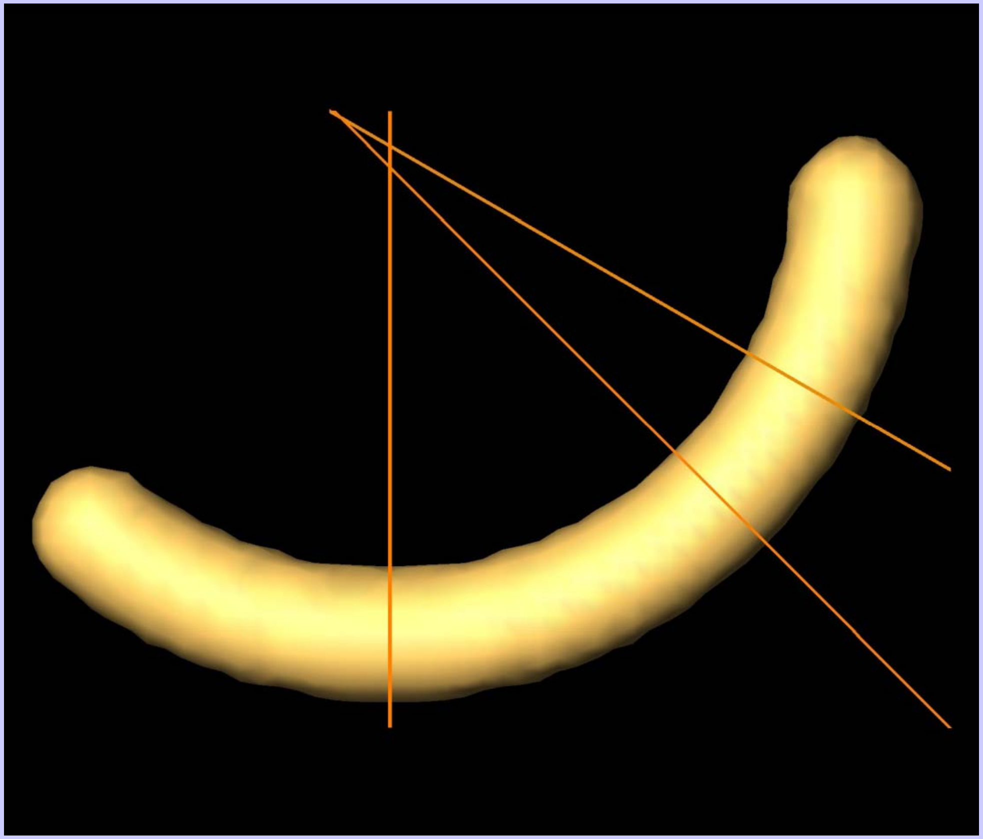

Examples of synthetic dendrites

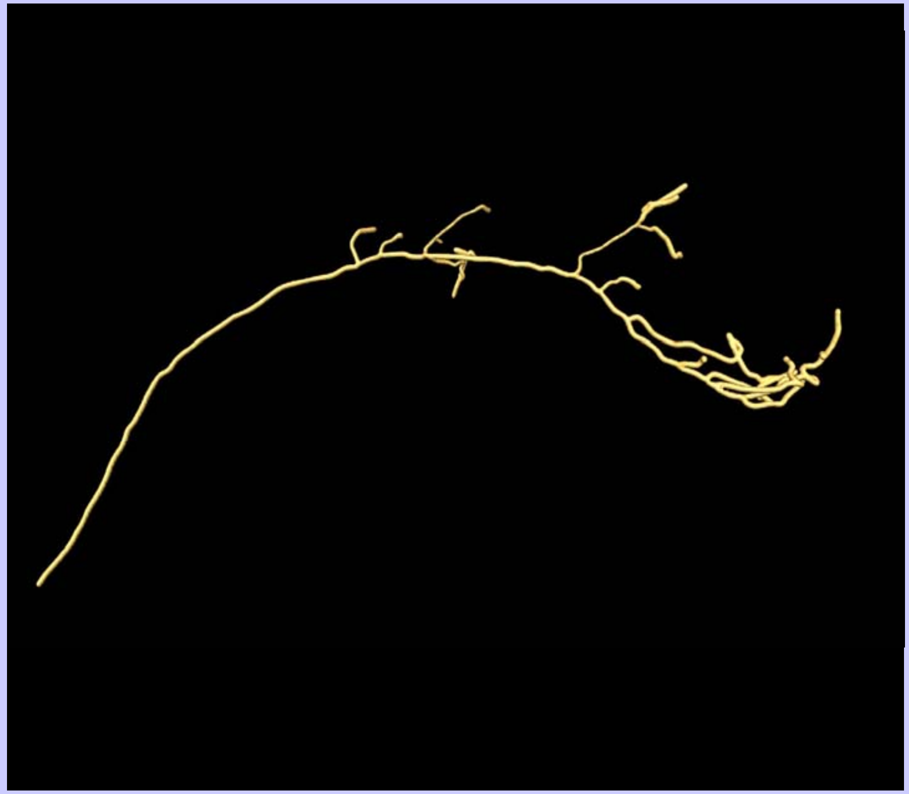

Thank you for attending

I thank the organizers for this wonderful meeting.

Thank the weather for the NFFFT 2011